

## A Study On Recent Trends In High Subsonic Flow Over Delta Wings .

Vishnu G Nair\*, Dileep M V\*\*, Prahlad K R\*\*\*

\*(Department of Aeronautical Engineering, MIT, Manipal,)

\*\* (Department of Instrumentation and Control Engineering, MIT, Manipal.)

\*\*\* (Department of Instrumentation and Control Engineering, MIT, Manipal.

### ABSTRACT

An understanding of the vortical structures and vortex breakdown is essential for the development of highly maneuverable and high angle of attack flight. This is primarily due to the physical limits these phenomena impose on aircraft and missiles at extreme flight conditions. In today's competitive world, demands for more maneuverable and stealthy air vehicles have encouraged the development of new control concepts for separated flows and vortex flow. An overview is given about investigations on a  $65^\circ$  delta wing using the Pressure Sensitive Paint (PSP) and Particle Image Velocimetry (PIV) techniques, carried out in the framework of Vortex flow experiment. For the delta wing with rounded leading edges and subsonic flow, the occurrence of a flat vortical structure as well as the onset of the primary vortex and the development of a vortex system consisting of an inner and outer vortex is described in dependency of the angle of attack and the Reynolds number. The  $Q$  - criterion is applied to the measured velocity data to estimate the circulation strength of individual vortices allowing for a quantitative description of the vortex developments and interactions. Furthermore, a case at transonic flow speeds ( $M = 0.8$ ) is described, showing a sudden occurrence of vortex breakdown above the delta wing, most probably induced by a shock wave. Vortex Flow Experiment provided a variety of experimental data for a  $65^\circ$  swept delta wing sharp and blunt leading edges. Flow details including forces and moments, surface pressures, Pressure Sensitive Paint measurements, and off-surface flow variables from Particle Image Velocimetry were made available for comparisons with computational simulations. This paper concentrates on some typical problems of delta wings with rounded leading edges at subsonic speed: the prediction of the main leading edge separation, the generation of the second inner vortex, the effect of transition, and Reynolds number effects.

*Keywords* – Subsonic flow ,delta wing, Vortex flow .

### I. INTRODUCTION

The delta wing flow field is dominated by vortical structures, the most prominent called leading-edge vortices. As angle of attack increases, these leading-edge vortices experience a sudden disorganization, known as vortex breakdown which can be described by a rapid deceleration of both the axial and swirl components of the mean velocity and, at the same time, a dramatic expansion of the vortex core. In the case of simple sharp edged delta wings, the flow separates along the whole leading edge already at small angles of attack. The shear layer rolls up forming strong vortices on the upper side of the wing, starting close to the wing apex and increasing in size and strength towards the wing aft. For delta wings with rounded leading edges, the flow topology can become more complicated. The flow separations are no longer fixed at the leading edge and their onset is delayed to higher angles of attack, depending on the shape of the leading edges, the Reynolds and Mach number. Furthermore, regions of attached flow around the leading edge can exist along with partly separated flow regions

resulting in multiple vortex systems. The generation of an apex and leading edge vortex was observed, for example, on a UCAV configuration with varying leading edge radius. But even in cases of simple delta wing geometries, i.e. straight leading with constant radius, complex vortex systems were observed, as shown for the present delta wing configuration

### II. TEST CONDITIONS AND DATA EVALUATION

#### Delta wing model geometry

The delta wing geometry used is a NASA delta wing of  $65^\circ$  sweep angle (Fig. 1). The geometry corresponds to a flat plate with curved leading and trailing edge sections, of which thickness distributions are described by polynomial formulas. Four different leading edge shapes are defined with increasing leading edge radius. For the tests in the transonic wind tunnel the 3/4 scale model ( $c_r = 0.4902$  m,  $b = 0.4572$  m,  $c = 0.3268$

m) was provided by NASA. The sharp as well as a leading edge with medium radius ( $r_{LE}/c = 0.0015$ ) were used for the present investigations.

### Transonic wind tunnel

The tests were carried out in the Transonic Wind tunnel (continuously running closed-circuit wind tunnel ) The test section of  $1\text{ m} \times 1\text{ m}$  size is enclosed by a plenum chamber, within which the total pressure can be set in a range from 30 000 to 150 000 Pa, so that Reynolds and Mach number effects can be studied independently. Different test sections are available enabling sub-, trans- and supersonic flow conditions. The perforated test section is used here, because small observation windows can be installed in the upper and lower wall behind which the PSP cameras and light sources are positioned. The walls of the perforated test section incorporate 60 degree inclined holes of 10 mm diameter, giving a porosity of 5.6%. However, no suction was applied during the tests. The top and bottom wall of the test section are inclined, i.e.  $\pm 0.25^\circ$  and  $\pm 0.563^\circ$  for  $M = 0.4$  and  $M = 0.8$  respectively, such that the cross section size increases downstream in order to compensate for the increasing boundary layer at the walls. The lateral walls were equipped with 50 mm thick schlieren windows of size  $450\text{ mm} \times 950\text{ mm}$ , hence enabling good optical access for PIV.

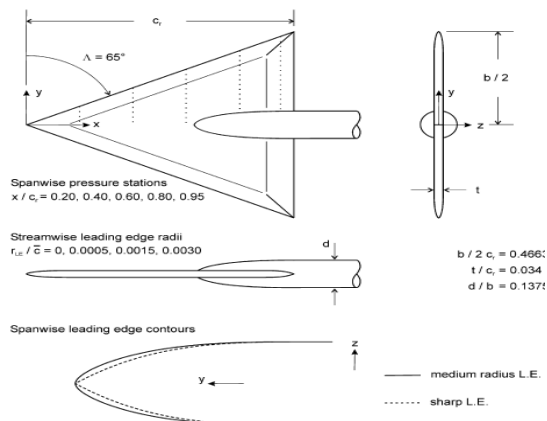
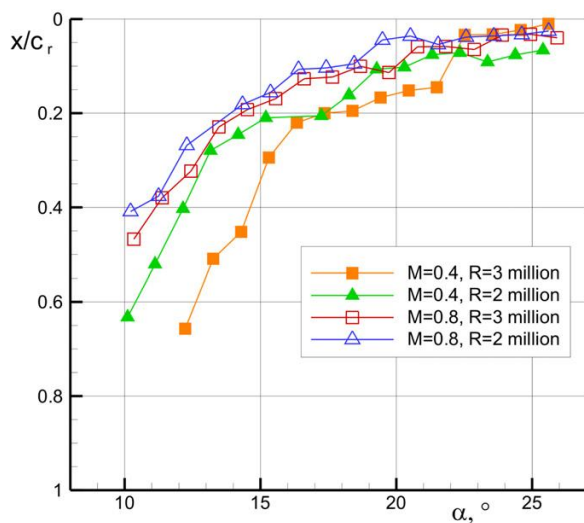


Fig.1. Delta wing geometry

### III. Result Analysis

For delta wings with sharp leading edges, the flow separates at the leading edges already at small angles of attack. The shear layer rolls up and the flow re-attaches to the model surface. The primary vortices are formed, starting at the apex of the delta wing. Depending on the angle of attack the attachment line is located at the center line of the delta wing or at a spanwise location between the primary vortex and the delta wing center line. Underneath the primary vortices an outboard directed flow establishes. If this flow passes the

suction peak, the steep adverse pressure gradient causes another flow separation and a counter-rotating secondary vortex is formed. In the case of rounded leading edges the flow separation is no longer fixed to the leading edge. The onset of the primary vortex becomes dependent on the leading edge radius, the angle of attack, the Reynolds and the Mach numbers. With increasing angle of attack the flow at the leading edge first separates on the rear part of the wing, where the ratio between the leading edge radius and the local wing span is small. The onset of the primary vortex occurs at a specific incidence when the flow separates effectively. Its origin moves upstream with increasing angle of attack until it reaches the wing apex. In Fig. 2 the pressure distribution is shown for the delta wing with sharp and medium radius leading edges. The suction peaks of the primary vortices are clearly visible, that start in the rounded leading edge case at  $x/cr = 0.6$  and in the case of the sharp edged delta wing at the wing apex. Using the PSP results, the chord locations of the primary vortex origins are determined at the starboard side of the wing. The results are plotted in Fig. 4 against  $\alpha$  in dependency of the Mach and Reynolds number. For  $M = 0.4$  and  $R_{mac} = 3$  million the onset of the primary vortex first takes place between  $\alpha = 11.2^\circ$  and  $12.3^\circ$ . Its origin is located at about  $x/cr = 0.65$  for  $\alpha = 12.3^\circ$ . After onset, the vortex origin moves quickly towards the wing apex with increasing angle of attack until a chord position of about  $x/cr = 0.3$  is reached; i.e.  $\alpha = 15.3^\circ$ . Passing this chord position the vortex origin moves more gradually upstream and asymptotically approaches a location close to the wing apex. The plot of  $M = 0.4$  and  $R_{mac} = 2$  million in Fig. 4 has a similar slope, however, shifted to lower angles of attack by about  $2^\circ$  showing that the onset of the primary vortex is postponed for higher Reynolds numbers. The plots for the transonic cases show that the Mach number has an opposite effect on the vortex onset. Also, the differences between both curves of  $R_{mac} = 2$  and 3 million is marginal for  $M = 0.8$  in comparison to the subsonic case. The gradients of the curves, particularly for  $M = 0.4$ , show that the location of the primary vortex is very sensitive to small changes of angle-of-attack for chord positions larger than  $x/cr = 0.3$ .



**Fig. 2.** Origin positions of primary vortex for  $\alpha > 10^\circ$  obtained from PSP results for the delta wing with medium radius leading edge for  $M = 0.4$  and  $0.8$  and  $R_{mac} = 2$  and  $3$  million

For the VFE-2 delta wing with rounded leading edges another vortex develops inboard of the leading edge. Fig. 5 shows the PSP results for  $M = 0.4$ ,  $R_{mac} = 3$  million and  $\alpha = 10.2^\circ$ . In this case the onset of the primary vortex takes place first at an angle of attack between  $11.2^\circ$  and  $12.2^\circ$ . The pressure distributions in Fig. 3, however, show a suction peak located inboard of the leading edge. In difference to the footprint of a primary vortex (see Fig. 3), this suction peak forms a line parallel to the leading edge with increasing peak height towards the trailing edge. Fig. 5 shows also the corresponding PIV results at a chord station of  $x/c_r = 0.6$ . The time averaged flow field shows close to the model surface a flat vortical structure spreading in the spanwise direction with a peak inboard of the leading edge. The corresponding  $Q$ -value distribution reveals that this structure consists of several discrete vortices as indicated in Fig. 3. Particularly, the outboard located vortices are fed with vorticity from the outer flow. Mainly these vortices produce the suction peak in the pressure distribution and increase in size and circulation strength further downstream. This inner vortical structure was not detectable for the delta wing with sharp leading edges which could be explained by the existence of the primary vortex starting at the apex just at small angles of attack that might inhibit the development of an inner vortical structure. However, inner vortices are also not detectable for the transonic cases ( $M = 0.8$ ) regardless of the leading edge radius.

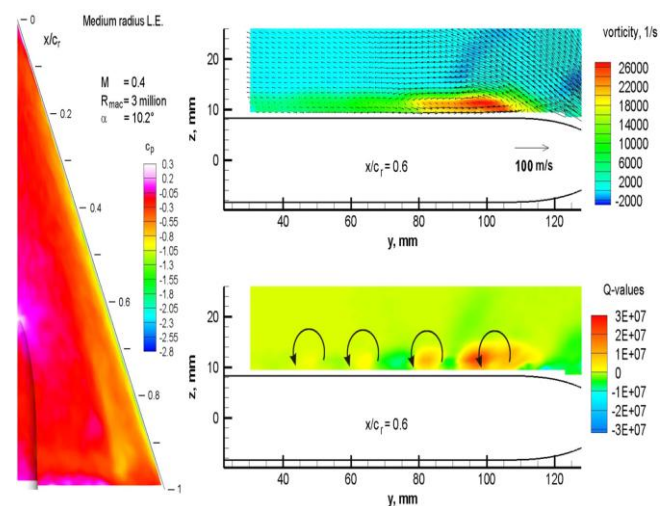


**Fig.3.** Time averaged PIV result at  $x/c_r = 0.6$  above the delta wing with medium radius leading edges and  $M = 0.4$ ,  $R_{mac} = 3$  million and  $\alpha = 10.2^\circ$  (top) velocity and vorticity distributions (bottom)  $Q$ -value distribution. The corresponding pressure distribution is shown on the left.

The flow topology above the delta wing with medium radius leading edges for  $M = 0.4$  and  $R_{mac} = 3$  million as discussed in the previous section changes at higher angles of attack, when the onset of the outer primary vortex takes place. This is in case the origin of the primary vortex is located at about  $x/c_r = 0.5$  for  $\alpha = 13.3^\circ$  (Fig. 5). Now, the footprint in the pressure distributions of the inner vortical structure has changed. Its maximum pressure peak height is reached just downstream of the origin of the outer primary vortex and drops down further downstream. In Fig. 5 the time averaged velocity is plotted above the delta wing in different planes. In the foremost shown chord station of  $x/c_r = 0.4$ , i.e. upstream of the origin of the primary vortex, the inner vortical structure can be seen again as a flat vortex close to the surface similar to the case at  $\alpha = 10.2^\circ$  as described in the former section. At the leading edge an attached flow exists, disregarding a possible flow separation bubble which cannot be resolved by the employed PIV setup. The velocity field at  $x/c_r = 0.5$  shows the flow field of the primary vortex close to its origin at the leading edge. Between the primary vortex and the inner vortical structure the flow reattaches to the surface and again separates due to the flow induced by the inner vortex. The inboard directed flow field in the vicinity of the inner vortices changes due to the developing primary vortex showing a more downward directed flow that seems to force a detachment of the inner vortices from the surface. This obviously leads to a merging of the inner co-rotating vortices and a single circular vortex is formed further downstream, which can be seen in

the velocity field at  $x/cr = 0.6$ . Now, two co-rotating vortices of approximately the same size can be observed; i.e. an inner and outer vortex. Between both vortices a reattachment and separation line exists at the surface. Further downstream the inner and outer vortices remain separated and do not merge (see Fig. 6,  $x/cr = 0.6$  to 0.8). With increasing size of the primary vortex a focus point is formed between the inner and outer vortex in the velocity field, so that at the surface an outboard directed flow establishes. In Fig. 7 the calculated circulations of the inner and outer vortices are plotted against the chord position for different Reynolds numbers and angles of attack. The dashed magenta line corresponds to the inner vortex for the current case. It shows that the circulation of the inner vortical structure first increases in the downstream direction until the primary vortex (solid magenta line) develops. However, not all the circulation possessed by the inner vortical structure is transferred to the newly formed inner vortex, as the negative step in the circulation curve between  $x/cr = 0.5$  and 0.6 indicates. This is also evidenced by the velocity field at  $x/cr = 0.7$  (Fig. 6), where small vortices can be detected inboard of the inner vortex. The circulation of the primary vortex continuously increases in a downstream direction (solid magenta line in Fig. 5), whereas the circulation of the inner vortex decreases slightly. Therefore, after the flow separates effectively at the leading edge vorticity is fed mainly to the primary vortex and no longer to the inner vortex.

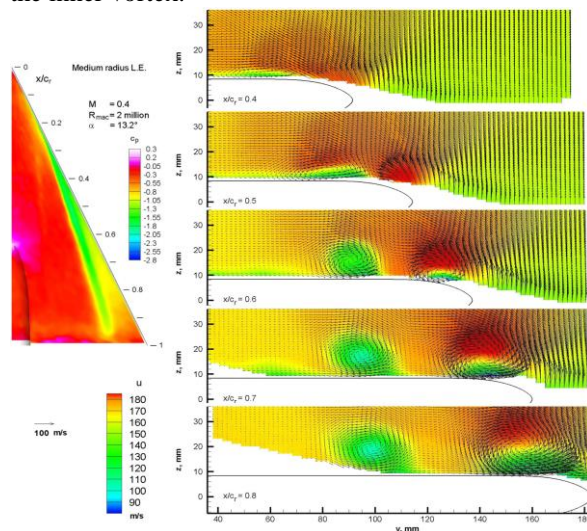


**Fig.4.** Surface pressure distributions obtained with PSP at suction side of delta wing with medium radius leading edges for different angles of attack ( $M = 0.4$ ,  $R_{mac} = 3$  million).

The origin of the outer primary vortex is also shifted upstream by reducing the Reynolds number which promotes the flow separation at the

leading edge. So, also a reduction of the Reynolds number indirectly lowers the circulation strength of the inner vortex for a specific angle of attack. From Fig. 5 it follows that the circulation is  $\Gamma = 1.4$  m<sup>2</sup>/s for  $R_{mac} = 3$  million and  $\alpha = 13.3^\circ$  (origin of the primary vortex:  $x/cr = 0.5$ ), which is about three times higher than that for the case of  $R_{mac} = 2$  million and  $\alpha = 13.2^\circ$ . Comparing the plots in Fig. 7 for  $R_{mac} = 2$  and 3 million at  $\alpha = 10.1^\circ$  and  $10.2^\circ$ , respectively, the circulation values of the inner vortical structure for  $x/cr$  0.6 are very similar, which shows the strength of the inner vortical structure to be less sensitive to the Reynolds number, i.e. if the primary vortex is not present. At the transonic speed of  $M = 0.8$  the flow is much more complex, because the flow above the delta wing reaches supersonic speeds and shock waves occur. Fig. 6 shows the pressure distributions for the sharp edged delta wing for different angles of attack. At  $\alpha = 24.1^\circ$  the footprints of the primary and secondary vortex originating from the wing apex are clearly visible. Plotted, are also constant lines of the sonic pressure coefficient  $c^*p$ . This shows that the outboard directed flow underneath the primary vortex close to the surface is supersonic, so that probably there is a cross-flow shock wave located in front of the secondary vortex. In Fig. 10 the velocity and vorticity distributions are plotted at  $x/cr = 0.6$  for an angle of attack of  $\alpha = 25.7^\circ$  showing the counter-rotating secondary vortex underneath the primary vortex. Also plotted are negative values of the divergence of the in-plane velocity vectors ( $\nabla \cdot v$ ) which gives an indication of the location and shape of a cross-flow shock wave. The contour lines of the sonic pressure coefficient in the center of the delta wing indicate the presence of a terminating shock wave in front of the sting fairing, i.e. at about  $x/cr = 0.55$ , and a second one closer to the trailing edge downstream of  $x/cr = 0.8$ .

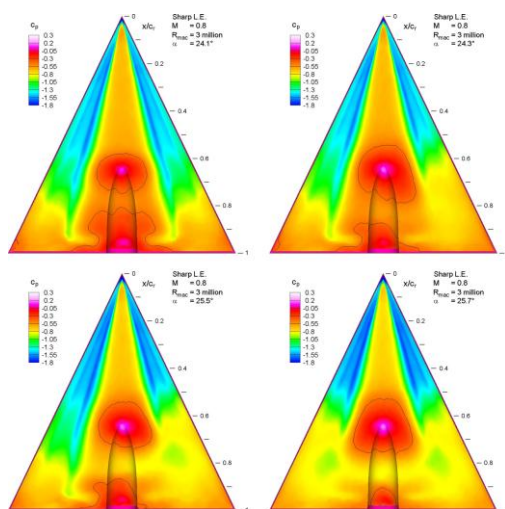


**Fig.5.** Surface pressure distributions obtained with PSP at suction side of delta wing with sharp leading edges in  $0.2^\circ$  steps of angles of attack ( $M = 0.8$ ,  $R_{mac} = 3$  million). The black contour lines indicate the sonic pressure coefficient  $c^*p = -0.43$

Increasing the angle of attack by only  $0.2^\circ$  the pressure distribution changes rapidly and becomes un-symmetric (see Fig. 5,  $\alpha = 24.3^\circ$ ). Following the suction peak of the primary vortex at the starboard side the peak enlarges suddenly downstream at a chord position of about  $x/cr = 0.7$  and the pressure increases. This suggests the occurrence of vortex breakdown, which may result from an interaction between the primary vortex and the terminating shock wave in front of the sting. This presumption is also proven by the fact that such an abrupt change of the pressure distribution does not occur in the subsonic cases as shown for example in Fig. 8 for the delta wing with rounded leading edges and an angle of attack of  $\alpha = 25.6^\circ$ . One must also note that this pressure change takes place by increasing the angle of attack by only  $\alpha = 0.2^\circ$ . However, the assumed vortex breakdown first occurs only at the starboard side of the wing, which shows that this flow situation seems to be very sensitive to small misalignments of the model or minor imperfections of the model geometry. The pressure distributions become again symmetric at an angle of attack of  $\alpha = 25.7^\circ$ . Again this takes place after an increase of angle of attack of only  $0.2^\circ$ , as shown in Fig. 5.

In Fig.6 the corresponding velocity distributions for  $\alpha = 25.7^\circ$  are plotted against the pressure distribution. The velocity field upstream of the presumed vortex breakdown is shown for  $x/cr = 0.55$ . The outward directed flow underneath the primary vortex separates at about  $y = 135$  mm ( $\eta = 0.85$ ) and a secondary vortex is formed. The flow field downstream the vortex breakdown at  $x/cr = 0.75$  shows a large region of reverse flow (up to  $u$

$= -60$  m/s), which is typically the case in the region of vortex breakdown.

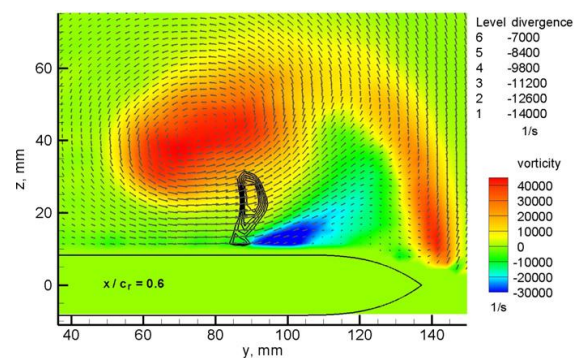


**Fig. 6.** Time averaged velocity and vorticity distributions for the delta wing with sharp leading edges at  $x/cr = 0.6$  ( $M = 0.8$ ,  $R_{mac} = 3$  million,  $\alpha = 25.7^\circ$ ). The color of the vectors corresponds to the out-of-plane vorticity

#### IV. CONCLUSION

An investigation of the flow topology above the VFE-2 delta wing was presented: surface pressure distributions were obtained using the Pressure Sensitive Paint technique and flow velocity fields using Particle Image Velocimetry. The analysis focused on the delta wing with rounded leading edges at a Mach number of 0.4, where an inboard vortex develops, and on a transonic case ( $M = 0.8$ ) which showed vortex breakdown. The onset of the primary vortex for rounded leading edges was analyzed in dependency of the Mach number, the Reynolds number ( $R_{mac} = 2$  and 3 million) and angles of attack ( $\alpha = 10^\circ - 25^\circ$ ). The Q-criterion could be applied to the PIV data to identify vortices and to calculate their circulation strength. At low angles of attack for  $M = 0.4$  and rounded leading edges, i.e. without a formation of a primary vortex, a flat vortical structure becomes visible close to the surface with an axis parallel to the leading edge. It could be shown, that this structure consists of several small scale co-rotating vortices. Their size and circulation strength increases towards the trailing edge. The strength seems to be less sensitive to the Reynolds number and increases with increasing angle of attack. This applies until onset of the primary vortex. When the primary vortex occurs, a more complex vortex system develops above the delta wing with rounded leading edges at  $M = 0.4$ . Upstream of the origin of the primary vortex the inner co-rotating vortical structure still exists. At the chord position of the primary vortex origin, vortices of this vortical structure detach from the surface and form a new vortex. This inner vortex does not merge further downstream with the co-rotating primary vortex. It was shown, that the circulation strength of the inner vortex depends strongly on the location of

the primary vortex. The inner vortex weakens when the primary vortex moves upstream, since vorticity is no longer fed into the inner vortical structure, where the primary vortex develops. For a Mach number of 0.8 the flow field above the delta wing reaches supersonic speeds, which leads to the formation of crossflow and terminating shock waves. The results at high angles of attack show a sudden change of the surface pressure within a range of increase of the angle of attack of only  $0.2^\circ$ . The velocity distributions show that a vortex breakdown occurs above the delta wing at about 65% of the root chord. This could be explained by an interaction between shock waves and the primary vortex. One terminating shock wave could be detected using the pressure distributions in front of the sting fairing; i.e. at about 55% of the root chord. The investigations on the VFE-2 show both measurement techniques to be powerful tools for flow analysis. However, the activities within VFE-2 also show useful interactions between computational and experimental disciplines. With the PSP result, showing the footprints of the inner and primary vortex, it was possible to provide parameters for a flow computation, which also predicted the inner vortex. In return, the CFD results were also useful in choosing the parameters of the PIV arrangement.

## REFERENCES

### Journal / Conference Papers

- [1] Robert Konrath, Christian Klein, Andreas Schroder, "PSP and PIV investigations on the VFE-2 configuration in sub- and transonic flow". 2012.
- [2] Willy Fritz. "Numerical simulation of the peculiar subsonic flow-field about the VFE-2 delta wing with rounded leading edge". 2012.

### Hand books

- [1] John D Anderson Jr., "Fundamentals of Aerodynamics", TMH.

### Web

- [1] [http://prezi.com/j\\_39bpgrlfmp/subsonic-flow-over-a-delta-wing/](http://prezi.com/j_39bpgrlfmp/subsonic-flow-over-a-delta-wing/)